

UNCLASSIFIED

Defense Technical Information Center
Compilation Part Notice

ADP012280

TITLE: Ferromagnetic and Structural Properties of Mn-Implanted p-GaN

DISTRIBUTION: Approved for public release, distribution unlimited

This paper is part of the following report:

TITLE: Applications of Ferromagnetic and Optical Materials, Storage and
Magnetoelectronics: Symposia Held in San Francisco, California, U.S.A. on
April 16-20, 2001

To order the complete compilation report, use: ADA402512

The component part is provided here to allow users access to individually authored sections
of proceedings, annals, symposia, etc. However, the component should be considered within
the context of the overall compilation report and not as a stand-alone technical report.

The following component part numbers comprise the compilation report:
ADP012260 thru ADP012329

UNCLASSIFIED

Ferromagnetic and Structural Properties of Mn-Implanted p-GaN

N. Theodoropoulou¹, A.F. Hebard¹, M.E. Overberg², C.R. Abernathy², S.J. Pearton², S.N.G. Chu³ and R.G. Wilson⁴

¹Department of Physics, University of Florida, Gainesville, FL 32611

²Department of Materials Science and Engineering, University of Florida, Gainesville, FL 32611

³Bell Laboratories, Lucent Technologies, Murray Hill, NJ 07974

⁴Consultant, Stevenson Ranch, CA 95131

ABSTRACT

High doses ($10^{15} - 5 \times 10^{16} \text{ cm}^{-2}$) of Mn^+ ions were implanted into p-GaN at $\sim 350^\circ\text{C}$ and annealed at $700\text{-}1000^\circ\text{C}$. At the high end of this dose range, platelet structures of $\text{Ga}_x\text{Mn}_{1-x}\text{N}$ were formed. The presence of these regions correlated with ferromagnetic behavior in the samples up to $\sim 250\text{K}$. At low doses, the implantation led to a buried band of defects at the end of the ion range.

There is tremendous interest in structures involving the manipulation of the spin of the electron in addition to its charge for switching and memory devices with new functionality.⁽¹⁻¹⁰⁾ Applications for these spintronic devices are envisioned in communications technology, data processing and storage and in photonics. It has been demonstrated in a number of semiconductors (including GaMnAs, InMnAs and ZnMnSe) that quantum spin states are quite robust and can be transported over very large distances ($>100 \mu\text{m}$ in some cases).⁽¹⁻¹⁰⁾ The ferromagnetism in dilute magnetic III-V semiconductors is carrier-induced and is still far from completely understood.^(11,12) The Curie temperature (T_C) in these materials is believed to be governed by the interaction between localized ferromagnetic clusters (bound magnetic polarons). Recent calculations⁽¹²⁾ suggest that wide bandgap semiconductors may have T_C values well above those for GaMnAs (110K)⁽¹⁰⁾ and InMnAs ($<35\text{K}$)⁽¹⁰⁾. In particular GaMnN with $\sim 5 \text{ at. \% Mn}$, and high hole concentrations is predicted to have a T_C exceeding 300K .⁽¹²⁾ At present, little is known about doping GaN with Mn, although some initial results have been published on n-type $\text{Ga}_x\text{Mn}_{1-x}\text{N}$ single crystallites with paramagnetic behavior.⁽¹³⁻¹⁵⁾

In this paper, we report on the magnetic properties of p-GaN implanted with high doses (3-5 at.%) of Mn. Under optimized annealing conditions we observe platelet regions with the same lattice structure as GaN, but different lattice constant, which give rise to Moiré fringes and multiple diffraction in transmission electron microscopy analysis. These regions, which appear to be $\text{Ga}_x\text{Mn}_{1-x}\text{N}$, produce ferromagnetic behavior with a T_C of $\sim 250\text{K}$. Thus, selected-area Mn-implantation into GaN may be useful for creating spin-injection contact regions.

The GaN samples were grown by Metal Organic Chemical Vapor Deposition on c-plane sapphire substrates. A low temperature (540°C) GaN buffer was grown first (250\AA) followed by $4\mu\text{m}$ of undoped GaN and $0.5\mu\text{m}$ of p-GaN (Mg-doped) with a room temperature hole concentration of $2 \times 10^{17} \text{ cm}^{-3}$. Mn^+ ions were implanted at an energy of 250keV and doses from $10^{15} - 5 \times 10^{16} \text{ cm}^{-2}$ at an approximate dose rate of $8 \times 10^{12} \text{ cm}^{-2} \cdot \text{s}^{-1}$ to produce average volume concentrations from $\sim 0.1\text{-}5 \text{ at. \%}$ in the top $\sim 2000\text{\AA}$ of the GaN. The samples were held at 350°C during implantation to avoid amorphization.⁽¹⁶⁻¹⁸⁾ Subsequent annealing at $700\text{-}1000^\circ\text{C}$ was performed for 5 mins under flowing N_2 gas with the samples face-down on GaN wafers. The

structural properties of the implanted material were examined by double crystal x-ray diffraction (XRD), and 200 kV transmission electron microscopy (TEM) with selected area diffraction analysis. The magnetic properties were measured in a Quantum Design PPMS SQUID magnetometer. The hole density after implantation and annealing was $\leq 10^{16} \text{ cm}^{-3}$.

Figure 1 shows TEM cross-sectional views of the GaN implanted with ~ 0.1 (top) or ~ 3 at.% Mn (center and bottom) and annealed at 700°C . For the low-dose case (top) the implanted regions contains a relatively large density of lattice defects resulting from agglomeration of point defects created by the nuclear stopping processes of the implanted ions. These samples showed only paramagnetic behavior. By sharp contrast, the samples implanted at higher doses show large ($\leq 200\text{\AA}$ diameter) platelet structures in addition to a buried band of damage at the end of range of the Mn ions. The end-of-range region is heavily-damaged single crystal. The platelet structures are shown in higher magnification at the bottom of Figure 1. Similar structures that were on average slightly larger in diameter ($\leq 250\text{\AA}$) were observed in the high dose samples annealed at 1000°C .

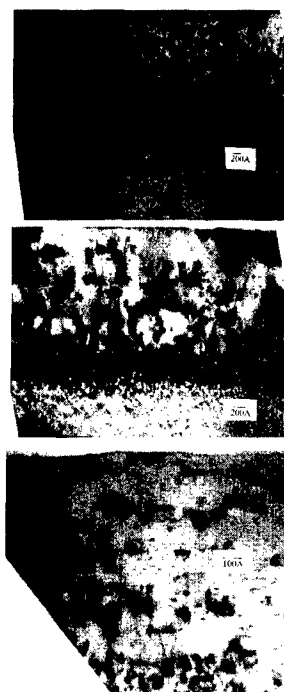


Figure 1. TEM micrographs taken under dark-field conditions of GaN after Mn^+ implantation and subsequent annealing at 700°C . The doses were 10^{15} cm^{-2} (top) or $5 \times 10^{16} \text{ cm}^{-2}$ (center and bottom) at 250 keV. The scales on the top two micrographs are 200\AA long, while in the bottom micrograph the scale is 100\AA long. The sample surface is at the top of each micrograph.

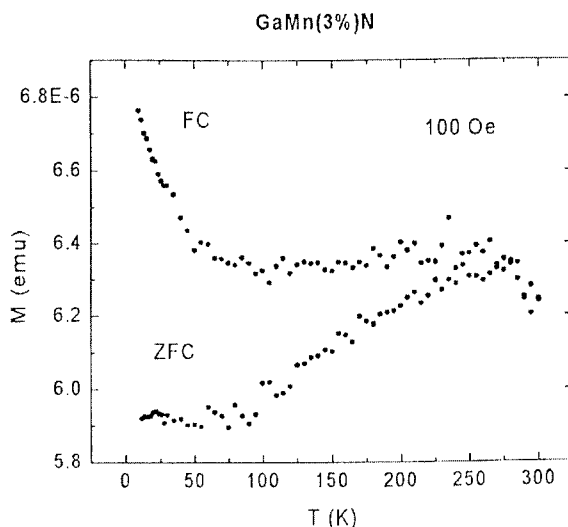


Figure 2. ZFC and FC magnetization as a function of temperature for GaN implanted with ~3 at. % Mn and annealed at 700°C.

The higher dose samples (≥ 3 at.% Mn) displayed a ferromagnetic behavior persisting to ~250 K as shown in Figure 2 for zero-field cooling (ZFC) and field-cooling (FC) conditions. There is also a contribution present with a Curie temperature of ~50 K, whose origin we have not identified. The difference between these plots essentially subtracts a large diamagnetic background. As further evidence of ferromagnetic behavior, Figure 3 shows that hysteresis was observed in the magnetic moment of the 3 at. % Mn sample. Assuming the ferromagnetism originates from the platelet structures, we can roughly estimate the saturation magnetization to be approximately 3.8 ± 1.3 Bohr magnetron per Mn. An alternative explanation could be that the GaMnN has a Curie temperature of 50 K, and superparamagnetic clusters of MnGa or some alloy thereof are present with size below the 20 Å resolution of TEM. The splitting of the FC/ZFC curve could then be attributed to the presence of these clusters with a blocking temperature of 250 K.

Numerous authors have reported on the creation of submicron MnGa and MnAs ferromagnetic crystallites in GaAs by Mn^+ implantation and subsequent heat treatment.⁽¹⁹⁻²³⁾ Both of these phases have T_C values above room temperature (eg. GaMn has T_C 's between 450-800 K depending on the amount of Mn in the alloy). In addition, ferromagnetic MnAs nanoclusters embedded in GaAs can be created by annealing of $\text{Ga}_{1-x}\text{Mn}_x\text{As}$ films.⁽²⁴⁾ In some cases, MnGa_xAs_y phases are observed in addition to the MnGa and MnAs phases⁽²³⁾, indicating that under some conditions it is possible to form ferromagnetic ternary phases. Note that for these GaAs experiments the Mn implants were performed at room temperature, in contrast to our use of elevated substrate temperatures which should reduce the point defect density.

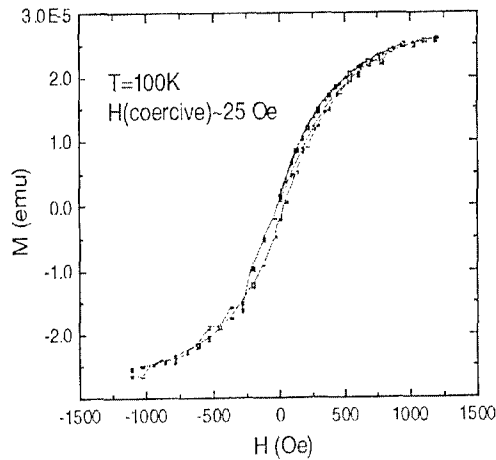


Figure 3. Hysteresis measured at 100K in the magnetic moment of a sample implanted with ~3 at. % Mn and annealed at 700°C.

Figure 4 shows a plan view TEM micrograph of a 5 at. % Mn implanted sample (top), along with selective area diffraction pattern (bottom). The sample was thinned from the backside and the data are typical of all samples implanted with 3-5 at. % Mn and annealed at 700°C or 1000°C. Electron diffraction did not show any 4-fold symmetry patterns, which would be expected to be present if either tetragonal (GaMn , $\text{Mn}_{0.6}\text{Ga}_{0.4}$, Mn_3N_2) or cubic (Ga_5Mn_8 , Mn_4N , $\text{Ga}_{7.7}\text{Mn}_{2.3}$) phases were formed. The diffraction pattern shows multiple diffraction spots around those of GaN with a 6-fold symmetry, indicating the platelet regions are $\text{Ga}_x\text{Mn}_{1-x}\text{N}$ with the same lattice structure as GaN but with a different (smaller) lattice constant which gives rise to the Moire fringes and multiple diffractions. This was confirmed by a qualitative simulation of [0001] double diffraction for a stack of two hcp lattices with different lattice constants, in analogy for a previous analysis of the cubic system GaAs on InP.⁽²⁵⁾ Similar diffraction results were obtained from cross-section samples, confirming that the Al_2O_3 substrates play no role. The only possible hexagonal phase present could be Mn_3Ga , but this was not found either in x-ray diffraction spectra or in energy dispersive x-ray spectroscopy analysis of the platelets. In the latter case, the probe beam was too large to get an exact composition for the platelets. Also, we could not apply Vegard's law due to the non-uniform composition in the Mn-implanted region. Moreover, we could expect the samples to display T_C values above room temperature if the binary GaMn phases were present.

In conclusion, high-dose Mn^+ implantation at elevated temperatures into p-GaN appears to be a promising method for producing ferromagnetic behavior and may be useful for creating selective-area spin-injection regions in device structures. The observed Curie temperature is below theoretical predictions, but may be affected by the low hole density in heavily implanted

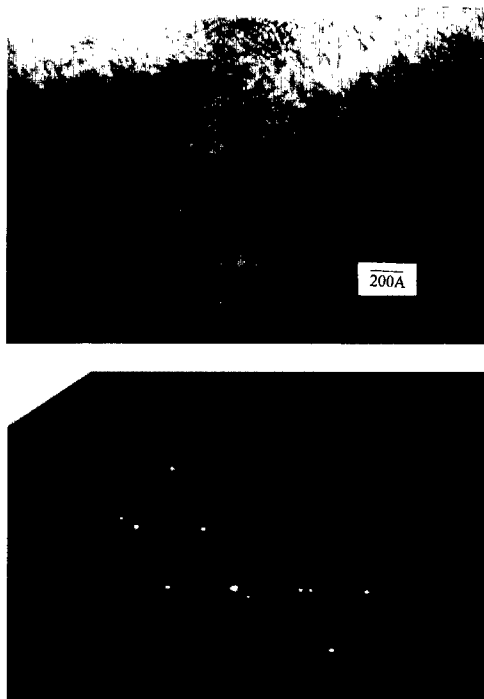


Figure 4. Plan view TEM micrograph of 5 at. % Mn-implanted GaN (dose $5 \times 10^{16} \text{ cm}^{-2}$ at 250 keV) sample annealed at 1000°C (top) and selected area diffraction pattern (bottom). The scale is 200Å long.

p-GaN. Considerable work needs to be done to understand the solubility limits of Mn under these conditions and the thermal stability of the phases created.

ACKNOWLEDGMENTS

The work at UF is partially supported by grants from AFOSR-MURI and NSF-DMR (97-32865), while that of RGW is supported by ARO (J.M. Zavada).

REFERENCES

1. D.D. Awschalom and J.M. Kikkawa, *Physics Today* **523**, 33 (1999).
2. J.M. Kikkawa and D.D. Awschalom, *Science* **287**, 473 (2000).
3. G.A. Prinz, *Science* **282**, 1660 (1998).
4. B.T. Jonker, Y.D. Park, B.R. Bennett, H.D. Cheong, G. Kioseoglou and A. Petrov, *Phys. Rev.* **B62**, 8180 (2000).
5. Y.D. Park, B.T. Jonker, B.R. Bennett, G. Itskos, M. Furis, G. Kioseoglou and A. Petrov, *Appl. Phys. Lett.* **77**, 3989 (2000).
6. F. Fiederling, M. Kelm, G. Reuscher, W. Ossau, G. Schmidt and A. Waag, *Nature* **402**, 787 (1999).
7. Y. Ohno, D.K. Young, B. Beschoten, F. Matsukura, H. Ohno and D.D. Awschalom, *Nature* **402**, 790 (1999).
8. an early review of the field is given in, F. Holtzberg, S. von Molnar and J.M.D. Coey, *Handbook of Semiconductors Vol. 3*, ed. S.P. Keller (North-Holland, Amsterdam 1980).
9. a review of hybrid ferromagnet-semiconductor research is given in M. Johnson, *IEEE Spectrum* **37**, 33 (2000); *J. Vac. Sci. Technol.* **A16**, 1806 (1998).
10. H. Ohno, *J. Mag. Mag. Mater.* **200**, 110 (1999).
11. J. König, H.H. Lin and A.H. MacDonald, *Phys. Rev. Lett.* **84**, 5628 (2000).
12. T. Diehl, H. Ohno, F. Matsukura, J. Cibert and D. Ferrand, *Science* **287**, 1019 (2000).
13. W. Gebicki, J. Strzeszewski, G. Kamler, T. Szczyko and S. Podsiado, *Appl. Phys. Lett.* **76**, 3870 (2000).
14. M. Zajac, R. Doradzinski, J. Gosk, T. Szczyko M. Palczewska, G. Grzanka, M. Lefeld-Sosnowska, W. Gebicki, M. Kaminska and T. Twardowski, *Appl. Phys. Lett.* **78**, 1276 (2001).
15. T. Szyszko, G. Kamler, B. Strojek, G. Weisbrod, S. Podsicask, L. Adamowicz, W. Gebicki, A. Twardowski, J. Szcztko and K. Sikorski (to be published).
16. S.O. Kucheyev, J.S. Williams, J. Zou, C. Jagadish and G. Li, *Appl. Phys. Lett.* **77**, 3577 (2000).
17. S.O. Kucheyev, J.S. Williams, C. Jagadish, V.S.J. Craig and G. Li, *Appl. Phys. Lett.* **78**, 1373 (2001).
18. S.O. Kucheyev, J.S. Williams, C. Jagadish, J. Zou and G. Li, *Phys. Rev.* **B62**, 75100(2000).
19. J. Shi, J.M. Kikkawa, R. Proksch, T. Schaeffer and D.D. Awschalom, *Nature* **377**, 707 (1995).
20. J. Shi, J.M. Kikkawa, D.D. Awschalom, G. Medeiro-Riberio, D.M. Petroff and K. Babcock, *J. Appl. Phys.* **79**, 5296 (1996).
21. J. DeBroeck, R. Osterholt, A. Van Euch, H. Bender, C. Brynseraede, C. Van Hoof and G. Borghs, *Appl. Phys. Lett.* **68**, 2744 (1996).
22. P.J. Wellman, J.M. Garcia, J.L. Feng and P.M. Petroff, *Appl. Phys. Lett.* **71**, 2532 (1997).
23. C. Chen, M. Cai, X. Wang, S. Xu, M. Zhang, X. Ding and Y. Sun, *J. Appl. Phys.* **87**, 5636 (2000).
24. H. Akinaga, S. Miyaniski, K. Tanaka, W. Van Roy and K. Onodera, *Appl. Phys. Lett.* **76**, 97 (2000).
25. S.N.G. Chu, *J. Appl. Phys.* **66**, 520 (1989).